Contents

1. Theoretical Background

This chapter provides a short introduction into Josephson junctions and their role in dc-SQUIDs[1], which will be the main focus of this thesis. We start with a brief overview on macroscopic quantum phenomena such as the Josephson effect and explain the general working principle of superconductor-isolator-superconductor (SIS) tunnel contacts, followed by a summary of their basic properties. They form the theoretical framework to describe the SQUIDs, which are developed in this group and optimized within the scope of this thesis. Lastly, we will take a closer look into their parasitic resonance behavior and investigate in the following chapter different methods to reduce the quality factors. The derivations of most equations were taken from the textbooks [Cla04] and [Gro16].

1.1 Josephson junctions

The *Josephson junction* named after Brian D. Josephson consists of two identical superconductors weakly coupled to each other. In the case of the junctions produced in this working group, such coupling is realized through a few nm thin insulating layer between the superconducting electrodes. Consequently, they are also referred to as SIS junctions. The resulting trilayer structure typically consists of Nb/Al-$\mathrm{AlO_x}$/Nb, with niobium being used for the superconductors and the insulating layer being provided by the aluminum oxide. A schematic structure is shown in figure 1.1. By connecting the tunnel junction to a current source they exhibit a non-trivial current-voltage behavior, which will be covered in the following.

1.1.1 Josephson effect

According to the BCS theory developed by Bardeen, Cooper and Schrieffer in 1957 [Bar57], electrons in a superconductor form pairs below a material dependent critical temperature T_c. These composite particles are also referred to as *Cooper pairs* and they represent the superconducting charge carriers with twice the mass and charge of a single electron. Their dissipationless flow causes the current to have zero dc-resistance, which is alongside the Meissner-Ochsenfeld effect [Mei33] the most characteristic feature of a superconductor. The latter describes magnetic field expulsion below T_c, provided the external magnetic field is smaller than a critical field

[1] **d**irect **c**urrent **S**uperconducting **QU**antum **I**nterference **D**evice

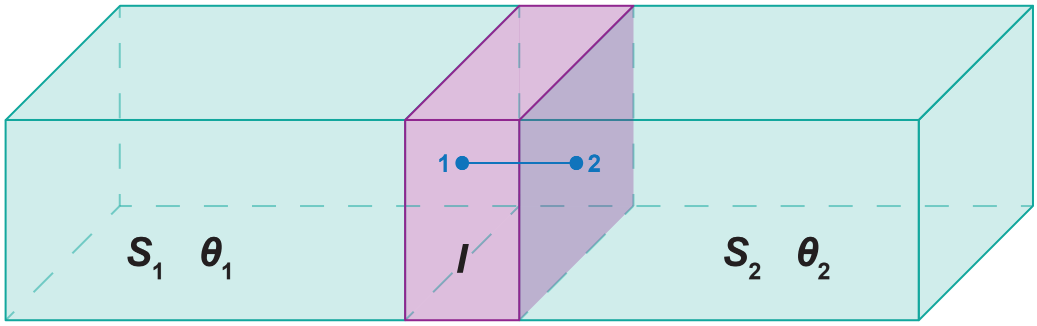

Figure 1.1: Schematic of a Josephson (SIS) junction. Both superconducting electrodes $\boldsymbol{S_1}$ and $\boldsymbol{S_2}$ are weakly coupled with each other through a thin tunnel barrier $\boldsymbol{I}$. $\boldsymbol{\theta_1}$ and $\boldsymbol{\theta_2}$ represent the macroscopic phases of each superconductor.

B_c. Further details on the microscopic theory of superconductivity can be found in [Bar57] and [Gin50].

If at $T < 4\,\mathrm{K}$ an external current source is connected to a Nb/Al-AlO$_x$/Nb Josephson junction, a supercurrent will flow despite the tunnel barrier, implying the tunneling of Cooper pairs as niobium is predominantly superconducting at these temperatures ($T_c = 9.3\,\mathrm{K}$ [Ina80]). Since the tunneling probability of an individual electron is approximately $p \lesssim 10^{-4}$ [Gro16], a much lower probability is to be expected for a Cooper pair consisting of two electrons. However, Josephson predicted that the tunneling behavior of Cooper pairs and individual conduction electrons must be the same. This is justified by the so-called *Macroscopic Quantum Model*, formulated by Fritz London in 1953.

The main focus here lies on the quantum mechanical phase θ. On one hand, the distance between both electrons in a Cooper pair is approximately 10 to 1000 nm which is significantly larger than the spacing between Cooper pairs, resulting in strongly overlapping wave functions. On the other hand, Cooper pairs have to obey Bose-Einstein statistics due to their total spin of 0. Thus, all Cooper pairs share the same ground state, and as a consequence, the energies and temporal evolutions of the phases are equal. These two effects lead to what is known as *phase-lock*. The phases of neighboring pairs synchronize such that this quantum mechanical property now holds on a macroscopic scale. This gives rise to a macroscopic wave function

$$\Psi(\mathbf{r},t) = \Psi_0(\mathbf{r},t)e^{i\theta(\mathbf{r},t)} \quad , \tag{1.1}$$

which describes all charge carriers of the superconductor. Here, the charge carrier density is given by $|\Psi_0(\mathbf{r},t)|^2 = n_s$. The time is denoted by t and $\mathbf{r}$ represents the position of the Cooper pair ensemble. As a result of sharing the same phase,

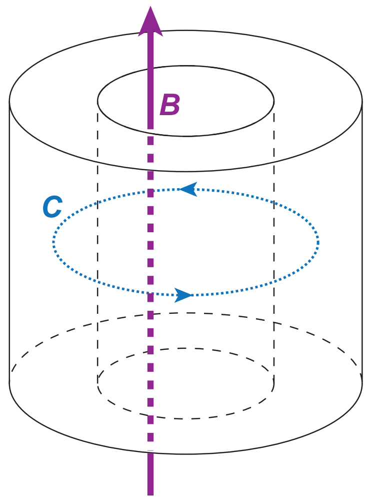

Figure 1.2: Superconducting ring-shaped cylinder threaded by an external magnetic field. By applying the field at low temperatures, shielding currents arise to expel the field from the superconductor. Upon turning off the external field the shielding currents will remain due to the lack of resistance, causing magnetic flux to be trapped. The dotted blue path C is situated at the center of the cylinder wall, which we assume to be current-free due to the London penetration depth λ_L being much smaller than the thickness of the cylinder wall.

both electrons of a Cooper pair consequently possess the same tunneling probability as an individual electron, enabling the supercurrent. This coherence phenomenon is referred to as the *Josephson effect* [Jos62]. Another significant consequence of the macroscopic quantum model is flux quantization. Together with the Josephson effect, this forms the basis for Josephson junctions and their applications.

Flux quantization is derived through the capture of an external magnetic flux within a superconducting cylinder (see figure 1.2). The wave function must remain unchanged after circumnavigating the cylinder due to $e^{i\theta} = e^{i\theta+2\pi n}$. As a result, upon integrating along the current-free center of the cylinder wall (path C), the following equation holds for the captured flux

$$\Phi = \frac{h}{q_\mathrm{s}} n = \frac{h}{2e} n \equiv \Phi_0 n \quad . \tag{1.2}$$

Here, $n \in \mathbb{Z}$ and $\Phi_0 = 2.07 \times 10^{-15}\,\mathrm{T\,m^2}$ [Tie21] represents the so-called magnetic flux quantum. The captured flux is thus quantized, a consequence solely arising from the macroscopic nature of the phase. This quantity plays a crucial role in the theoretical description of Josephson junctions.

The current and voltage behavior in a SIS junction is described by the *Josephson equations*. Crucial to this description is a critical current I_c that is linearly proportional to the applied current I, which marks the boundary between two operational modes; the zero-voltage state and the voltage state. Additionally, due to the macroscopic nature of the phase, I oscillates with the gauge-invariant phase difference φ, leading to the **first Josephson equation** [Jos65]

$$I_s = I_c \sin(\varphi) \quad . \tag{1.3}$$

I_c is proportional to the coupling strength κ, which describes the overlap of the wave functions Ψ_1 and Ψ_2 within the insulating layer. The relationship is given by

$$I_c = \frac{4e\kappa V n_s}{\hbar} \quad , \tag{1.4}$$

where V represents the volume of the superconducting electrode and e denotes the elementary charge of an electron. We assume that the Cooper pair density n_s of the two superconductors S_1 and S_2 is identical, meaning $n_{s1} = n_{s2} = n_s$.

The gauge-invariant phase difference refers to the phases θ_1 and θ_2 of the respective electrodes at the boundary of the insulating layer (positions 1 and 2, see figure 1.1). Taking into account possible external electromagnetic fields within the barrier, the general form using the vector potential **A** is given by [Gro16]

$$\varphi(\mathbf{r}, t) = \theta_2(\mathbf{r}, t) - \theta_1(\mathbf{r}, t) - \frac{2\pi}{\Phi_0} \int_1^2 \mathbf{A}(\mathbf{r}, t) \cdot \mathrm{d}\mathbf{l} \quad . \tag{1.5}$$

Assuming a constant supercurrent density J_s across the junction, taking the time derivative of equation (1.5) yields the **second Josephson equation** [Jos65]

$$\frac{\partial \varphi}{\partial t} = \frac{2\pi}{\Phi_0} V \quad . \tag{1.6}$$

The first operating mode describes the zero-voltage state, i.e. $I < I_c$ (zero-voltage state). Here, the entire injected current is carried by Cooper pairs, so $I = I_s = \text{const.}$ As a result, φ is constant over time, which, according to equation (1.6), leads to $V = 0$. This is known as the *dc Josephson effect.*

For $I > I_c$ however, Cooper pairs begin to break up such that a portion of the current needs to be carried by quasiparticles, which will then lead to a voltage drop V. According to the second Josephson equation, the phase φ becomes time dependent, and after integration one obtains

$$\varphi = \frac{2\pi}{\Phi_0} V t + \varphi_0 = w_J t + \varphi_0 \quad \text{with} \quad w_J = \frac{2\pi}{\Phi_0} V \quad . \tag{1.7}$$

Thus, if we insert equation (1.7) into equation (1.3), we observe that the current I_s oscillates with the *Josephson frequency* $\frac{f_J}{V} = \frac{w_J}{2\pi V} = \frac{1}{\Phi_0} \approx 483.6\,\frac{\text{MHz}}{\mu\text{V}}$. Accordingly, this phenomenon is referred to as the *ac Josephson effect.*

1.1.2 Josephson Junctions in a Magnetic Field

To motivate the structure of a dc-SQUID, it is essential to first investigate the current behavior of an extended Josephson junction in the presence of an external magnetic field. So far, all previous formulae apply for point-like junctions, assuming a spatially constant phase difference φ and Josephson current density J_s across the junction area. This is not the case for three-dimensional (extended) junctions with a length L and width W. The *Josephson penetration depth* λ_J is a quantity used to classify an extended junction as short $(\mathrm{W}, \mathrm{L} \leq \lambda_J)$ or long $(\mathrm{W}, \mathrm{L} \geq \lambda_J)$ and is defined as

$$\lambda_J = \sqrt{\frac{\Phi_0}{2\pi\mu_0 J_c t_B}} \quad . \tag{1.8}$$

Here, the magnetic thickness is defined as $t_B = d + \lambda_{L,1} + \lambda_{L,2}$. It describes how far an external magnetic field penetrates both superconducting electrodes if applied parallel

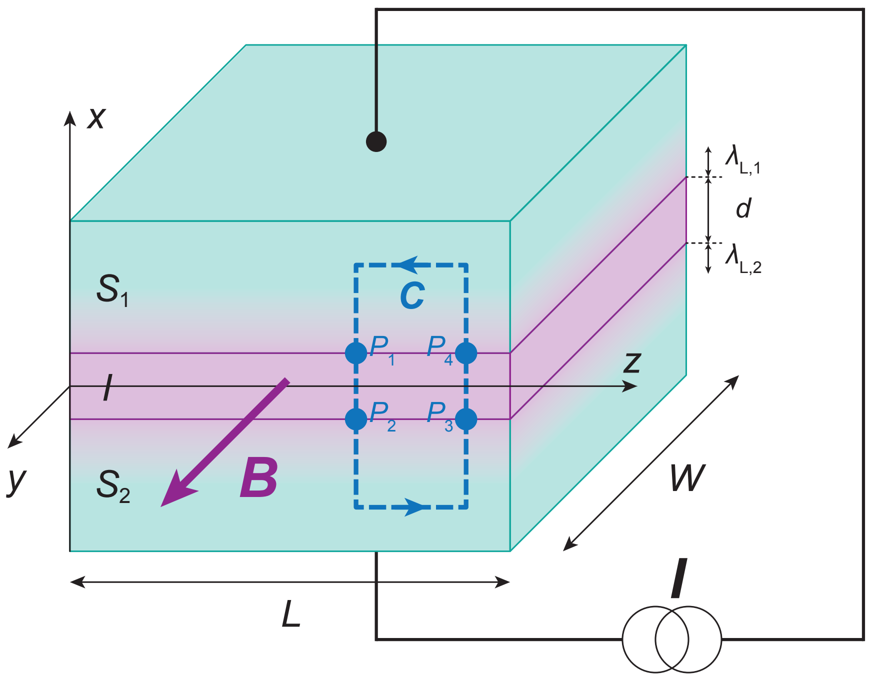

Figure 1.3: Short Josephson junction connected to a current source in the presence of an external B-field in y-direction, parallel to the junction area. Inside the electrodes the magnetic field decays exponentially according to the London penetration depths $\lambda_{L,1}$ and $\lambda_{L,2}$, visually shown by the purple color gradient. The closed contour C is used to derive expressions for the spatially dependent phase difference φ and current density J_s.

to the junction area, as depicted in figure 1.3. The respective London penetration depths are $\lambda_{\mathrm{L},1}$ and $\lambda_{\mathrm{L},2}$ and $J_\mathrm{c} = \frac{I_\mathrm{c}}{WL}$ is the critical current density. This distinction is needed to determine whether the magnetic self-field generated by the supercurrent is negligible in comparison to the external field (short junctions) or not (long junctions). Within the scope of this thesis, we only use short junctions.

To analyze the current and phase distribution of such a junction we consider the setup shown in figure 1.3. A short junction is connected to a current source and is penetrated by an external B-field in y-direction, parallel to the junction area. Now, obtaining an expression for the phase requires a similar approach as the calculation for the quantized flux, where we assumed that the phase changes by $2\pi n$ around a closed loop. Here, we again integrate over a closed contour C, with the points $P_1 - P_4$ marking the transitions between superconductor and isolator. Using equation 1.5, we find

$$\frac{\partial \varphi}{\partial z} = \frac{2\pi}{\Phi_0} B_\mathrm{y} t_\mathrm{B} \quad \text{and} \quad \frac{\partial \varphi}{\partial y} = -\frac{2\pi}{\Phi_0} B_\mathrm{z} t_\mathrm{B} \quad . \tag{1.9}$$

In this experiment, however, the magnetic field points in y-direction only, meaning φ will only vary along the z-axis. Integrating the first expression in equation 1.9 then leads to

$$\varphi(z) = \frac{2\pi}{\Phi_0} B_\mathrm{y} t_\mathrm{B} z + \varphi_0 \quad . \tag{1.10}$$

Here, the integration constant φ_0 represents the phase difference for the case $z = 0$. Inserting equation 1.10 into the first Josephson equation and using $J_\mathrm{s} = \frac{I_\mathrm{s}}{WL}$ gives

$$J_\mathrm{s}(y, z, t) = J_\mathrm{c}(y, z) \sin(kz + \varphi_0) \quad \text{with} \quad k = \frac{2\pi}{\Phi_0} B_\mathrm{y} t_\mathrm{B} \quad . \tag{1.11}$$

If we now assume the critical current density J_c to be constant across the junction area, we can integrate equation 1.11 to get a flux-dependent maximum Josephson current

$$I_\mathrm{s}^\mathrm{m}(\Phi) = I_\mathrm{c} \left| \frac{\sin(\frac{kL}{2})}{\frac{kL}{2}} \right| = I_\mathrm{c} \left| \frac{\sin(\frac{\pi\Phi}{\Phi_0})}{\frac{\pi\Phi}{\Phi_0}} \right| \quad . \tag{1.12}$$

This expression describes the so-called Fraunhofer diffraction pattern, shown in figure 1.4. The result resembles the single slit experiment, where the same pattern is found for the light intensity behind the slit. Here, the analogy works by considering the integral of the critical current density J_c as a transmission function which is constant inside the junction and zero outside.

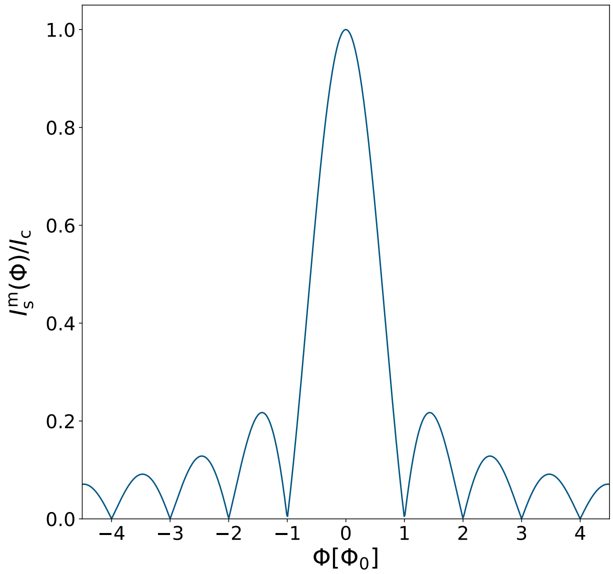

Figure 1.4: Normalized flux-dependent maximum Josephson current $I_\mathrm{s}^\mathrm{m}(\Phi)$ showing a Fraunhofer pattern. It modulates with the flux quantum Φ_0, peaking at $\Phi = 0$ with subsequent maxima at $\Phi = \pm(\frac{3}{2} + n)\Phi_0$ with $n \in \mathbb{N}_0$. For $\Phi = \pm(n+1)\Phi_0$ the total net current is zero.

1.1.3 RCSJ Model

Until now, we investigated the current-voltage behavior under the assumption of $I < I_\mathrm{c}$, staying in the so-called zero-voltage state. In this regime, only the dc Josephson effect applies as discussed in subsection 1.1.1. Switching to the voltage stage, i.e. $I > I_\mathrm{c}$, Cooper pairs start breaking up into quasiparticles if the electric energy eV exceeds the sum of both electrodes' gap energies $\Delta_1(T) + \Delta_2(T)$. Consequently, at the *gap-voltage*

$$V_\mathrm{g} = \frac{\Delta_1(T) + \Delta_2(T)}{e} \tag{1.13}$$

quasiparticles start to cross the tunnel barrier resulting in a steep rise of a resistive normal current I_n. This process also occurs at finite temperatures for $k_\mathrm{B}T > \Delta_1(T) + \Delta_2(T)$, leading to a reduction of I_c as well as V_g. Under a current source, the condition $I = I_\mathrm{s} + I_\mathrm{n}$ must be constantly fulfilled. This results in an oscillating normal current, since I_s oscillates with f_J according to the ac Josephson effect. The time evolution of the phase difference $\frac{\mathrm{d}\varphi}{\mathrm{d}t}$ will therefore vary sinusoidally, causing both I_s and I_n and the resulting voltage to oscillate in a complex manner. As a voltage with such a high frequency cannot be measured, only the time-averaged voltage will be considered in the following discussion.

Now, further increasing the energy of the quasiparticles ($T > T_\mathrm{c}$ and/or $V > V_\mathrm{g}$) leads to a transition into normal-conducting electrons, which exhibit an ohmic dependence. This behavior can be seen in the typical current-voltage-characteristic

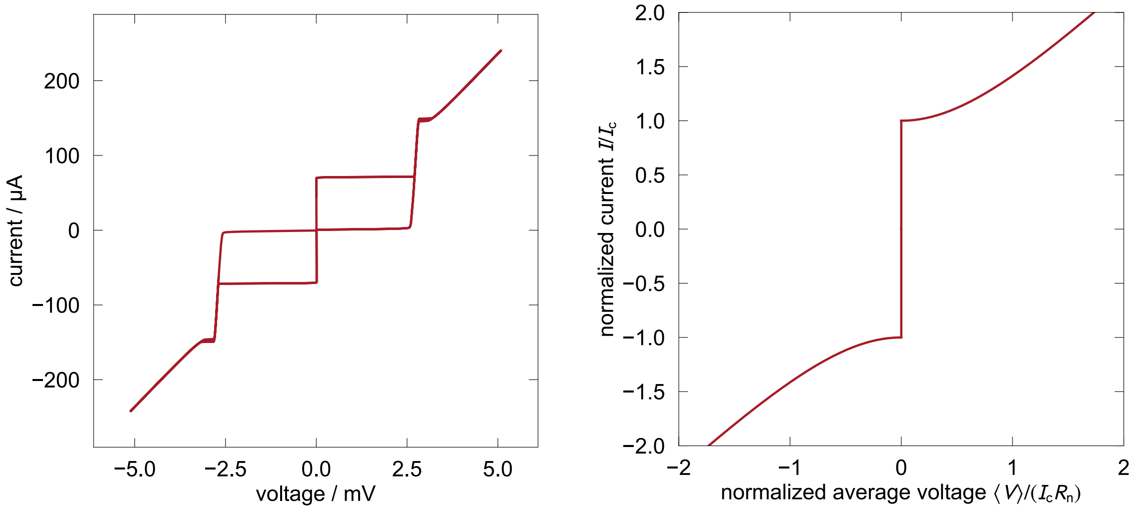

Figure 1.5: Platzhalter Plots von Alex -> eigene Messung vornehmen?... Measured IVCs from cross-type junctions manufactured in this working group. Left: Underdamped junction showing the typical hysteresis. Right: Overdamped junction with a current-voltage shape that is independent of the current sweep direction.

(IVC) depicted in figure 1.5.

The junctions produced in this working group, however, are comprised of two electrodes separated by a thin insulating layer, which represent a parallel plate capacitor with the Al-$\mathrm{AlO_x}$ layer being the dielectric material. Therefore, a junction capacitance C needs to be taken into account. A displacement current I_d will flow as a consequence, given we are in the voltage state. Lastly, thermal and 1/f noise cause a small fluctuating current I_f. All these current channels were defined in the so-called Resistively and Capacitively Shunted Junction (RCSJ) model [McC68], [Ste68], which models the total current of a lumped (0-dimensional) junction to a sufficiently high accuracy. A schematic of an effective circuit diagram is shown in figure 1.6 (left). Combining every current channel leads to the *Basic Junction Equation*, which is defined as [Gro16]

$$I = I_\mathrm{s} + I_\mathrm{n} + I_\mathrm{d} + I_\mathrm{f} = I_\mathrm{c}\sin(\varphi) + \frac{1}{R(V)}\frac{\Phi_0}{2\pi}\frac{\mathrm{d}\varphi}{\mathrm{d}t} + C\frac{\Phi_0}{2\pi}\frac{\mathrm{d}^2\varphi}{\mathrm{d}t^2} + I_\mathrm{f} \quad . \tag{1.14}$$

By defining the Josephson coupling energy $U_{\mathrm{J}0} = \frac{\hbar I_\mathrm{c}}{2e}$ and the normalized currents $i = \frac{I}{I_\mathrm{c}}$ and $i_\mathrm{f}(t) = \frac{I_\mathrm{f}(t)}{I_\mathrm{c}}$, equation 1.14 can be rewritten to

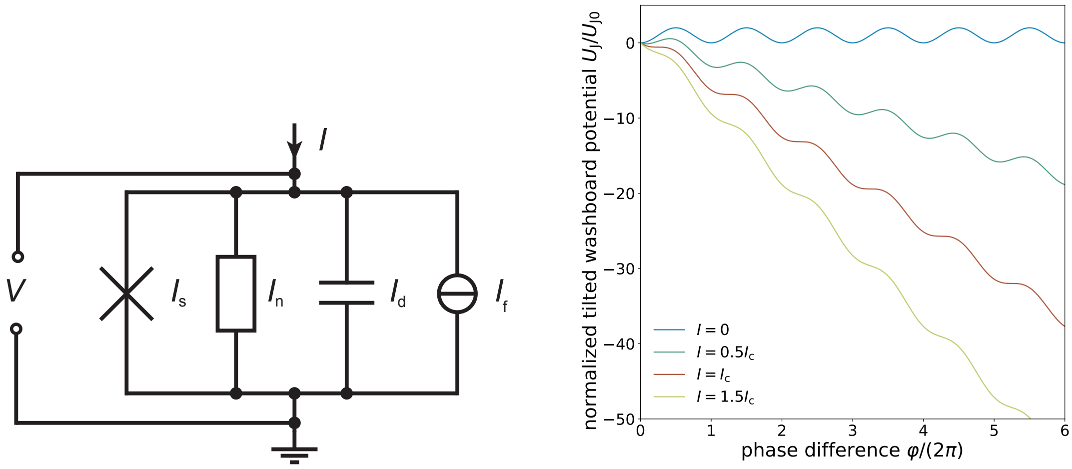

Figure 1.6: Left: Schematic circuit of a lumped Josephson junction with all four current channels connected in parallel, according to the RCSJ model. The junction is represented by the cross symbol on the left, marking the supercurrent I_s. The normal current I_n is realized with a resistance R, while the displacement current I_d and the noise I_f need a capacitor C and a current source, respectively. Right: Tilted washboard potential for different currents, ranging from 0 to $1.5I_\mathrm{c}$. The tilt increases with the injected current I.

$$\left(\frac{\hbar}{2e}\right)^2 C\frac{\mathrm{d}^2\varphi}{\mathrm{d}t^2} + \left(\frac{\hbar}{2e}\right)^2 \frac{1}{R(V)}\frac{\mathrm{d}\varphi}{\mathrm{d}t} + \frac{\mathrm{d}}{\mathrm{d}\varphi}\left\{U_{\mathrm{J0}}\left[1-\cos\varphi - i\varphi + i_\mathrm{f}(t)\varphi\right]\right\} = 0 \quad . \tag{1.15}$$

The expression in the curly brackets represents the potential energy in the system U_J, allowing equation 1.14 to be compared to

$$M\frac{\mathrm{d}^2x}{\mathrm{d}t^2} + \eta\frac{\mathrm{d}x}{\mathrm{d}t} + \nabla U = 0 \quad . \tag{1.16}$$

This equation describes a particle with mass M and damping η moving inside the potential U. The mechanical analogue therefore allows us to interpret a *phase particle*, where it's motion corresponds to a change of the gauge-invariant phase difference φ within a potential U_J [Cla04]. Consequently, it is attributed with a mass $M = \left(\frac{\hbar}{2e}\right)^2 C$ and damping $\eta = \left(\frac{\hbar}{2e}\right)^2 \frac{1}{R(V)}$. Figure 1.6 (right) visualizes how this phase particle behaves for different currents I. Given the shape of $U_\mathrm{J}(\varphi)$, the potential is referred to as the *tilted washboard potential*.

For $I = 0$, the phase particle will remain within one of the potential minima. As the current increases, however, the potential starts to tilt such that the depth of the minima reduces until it vanishes for $I = I_c$, thus becoming a saddle point. Up until this point, the phase particle can't overcome the potential barrier to move downward, which confirms the second Josephson equation as the phase difference φ should remain constant on average for $I < I_c$. Further increasing the current and therefore the tilt of the potential causes the phase particle to fall along the potential, resulting in a voltage drop across the junction ($\frac{\partial\varphi}{\partial t} > 0$).

Reversing the current sweep showcases the importance of the particle's mass M and damping η, as they determine if the return path equals the above described current shape or not. For the case of a small mass (small C) and large damping (small R), the phase particle will, due to a lack of momentum, come to a halt as soon as minima reappear in the washboard potential by reducing the current below I_c. The current path will therefore remain unchanged as I is reduced back to 0, as shown in figure 1.5 (right). Such a junction is consequently called an *overdamped* junction.
The other case describes an *underdamped* junction (figure 1.5 (left)) and involves a large mass (large C) and small damping (large R). This allows the phase particle to continue to move downward as it now carries enough momentum to overcome the arising maxima and minima. The finite voltage drop despite the current being below I_c is displayed as the steep quasiparticle current curve, which ends with a return current I_R that arises with the recapture of the particle in a minimum. This leads to a hysteretic IVC, as depicted in figure 1.5 (left). I_R can be calculated via [Lik86]

$$I_\mathrm{R} = \frac{4}{\pi\sqrt{\beta_\mathrm{C}}} I_\mathrm{c} \quad , \tag{1.17}$$

with β_C being the dimensionless Stewart-McCumber parameter, that is used to quantitatively distinguish between both junction types. It is given by

$$\beta_\mathrm{C} = \frac{2\pi}{\Phi_0} I_\mathrm{c} R^2 C \tag{1.18}$$

with $\beta_C \gg 1$ corresponding to a strongly underdamped junction, whereas $\beta_C \ll 1$ represents a strongly overdamped junction. The junctions developed and produced within the scope of this thesis aim to be overdamped, which is why we take a closer look on the time-averaged voltage for $I > I_c$ in the case of $\beta_C \ll 1$. Neglecting the noise in equation 1.15, as well as assuming the resistance to be linear below and above the gap voltage V_g, i.e. $R(V) = R$, the time-averaged voltage can be derived to [Cla04]

$$\langle V(t) \rangle = I_c R \sqrt{\left(\frac{I}{I_c}\right)^2 - 1} \quad \text{for} \quad \frac{I}{I_c} > 1 \quad . \tag{1.19}$$

This equation will be crucial to determine the voltage drop of a dc-SQUID, as its derivation is analogous to that of a single junction, which will be covered in the next section.

1.2 dc-SQUIDs

We have now covered the theoretical framework necessary to understand the working principle of a dc-SQUID, which consists of a superconducting ring intersected by two identical Josephson junctions with critical Josephson currents I_c, as depicted in figure 1.7. Both junctions are shunted with shunt resistors R_s to avoid hysteretic behavior in the respective IVCs. If the loop is then biased with a bias current I_b while being threaded by an external magnetic flux Φ_e, it is possible to convert small flux variations into a measurable voltage change. dc-SQUIDs are therefore used as highly sensitive flux-to-voltage transducers.

1.2.1 Zero Voltage State

In order to fully understand the working principle of a dc-SQUID it is again necessary to first cover the zero voltage stage as we did for a single junction. The parallel connection of the two junctions allows the bias current to split into two supercurrents I_{s1}, I_{s2} with identical critical currents, i.e. $I_{c,1} = I_{c,2} = I_c$. Here we assume $I_b < 2I_c$

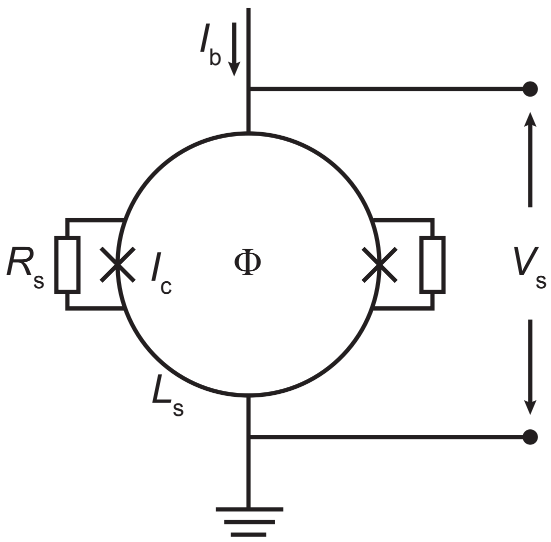

Figure 1.7: Schematic circuit diagram of a shunted dc-SQUID. A superconducting loop with inductance L_s is interrupted by two lumped Josephson junctions such that they form a parallel connection. Operation requires a bias current I_b and an external magnetic flux Φ. To avoid hysteresis effects, a shunt resistance R_s is connected to each junction.

to ensure that no voltage drop across both junctions occurs ($V_\mathrm{s} = 0$). Applying Kirchhoff's law we then obtain the following expression

$$I_\mathrm{b} = I_\mathrm{s} = I_\mathrm{c}\sin\varphi_1 + I_\mathrm{c}\sin\varphi_2 = 2I_\mathrm{c}\cos\left(\frac{\varphi_1-\varphi_2}{2}\right)\sin\left(\frac{\varphi_1+\varphi_2}{2}\right) \quad . \tag{1.20}$$

In chapter 1.1.2 we concluded that a magnetic flux Φ causes the supercurrent to modulate with Φ_0. A dc-SQUID can be considered as a single junction with a much larger effective area A_eff (loop area), that an external magnetic fux can penetrate. It is therefore reasonabe to expect a similar behavior for a dc-SQUID. The same approach as with a single junction is used to determine the flux dependency of the total supercurrent, where a closed loop integral is performed around the SQUID loop. The calculation leads to the relation [Gro16]

$$\varphi_2 - \varphi_1 = \frac{2\pi\Phi}{\Phi_0} \quad , \tag{1.21}$$

which can be directly inserted into equation 1.20 to obtain

$$I_\mathrm{s} = 2I_\mathrm{c}\cos\left(\pi\frac{\Phi}{\Phi_0}\right)\sin\left(\varphi_1 + \pi\frac{\Phi}{\Phi_0}\right) \quad . \tag{1.22}$$

In the most general case, however, one needs to take into account the inductance L_s of the SQUID loop and therefore a circulating current $I_\mathrm{cir} = \frac{I_\mathrm{s1}-I_\mathrm{s2}}{2}$ that induces the additional flux $\Phi_\mathrm{cir} = L_\mathrm{s}I_\mathrm{cir}$. With the external flux Φ_e we can thus write for the total flux

$$\begin{aligned}
\Phi &= \Phi_\mathrm{e} + \Phi_\mathrm{cir} && (1.23)\\
&= \Phi_\mathrm{e} - L_\mathrm{s}I_\mathrm{c}\sin\left(\pi\frac{\Phi}{\Phi_0}\right)\cos\left(\varphi_1 + \pi\frac{\Phi}{\Phi_0}\right) && (1.24)\\
&= \Phi_\mathrm{e} - \frac{1}{2}\beta_L\Phi_0\sin\left(\pi\frac{\Phi}{\Phi_0}\right)\cos\left(\varphi_1 + \pi\frac{\Phi}{\Phi_0}\right) \quad . && (1.25)
\end{aligned}$$

Here, we introduced the dimensionless screening parameter $\beta_\mathrm{L} = \frac{2L_\mathrm{s}I_\mathrm{c}}{\Phi_0}$, which relates the maximum possible flux $\Phi_\mathrm{cir}^\mathrm{max} = L_\mathrm{s}I_\mathrm{cir}^\mathrm{max} = L_\mathrm{s}I_\mathrm{c}$ produced by screening currents to $\frac{\Phi_0}{2}$. This quantity describes the influence the screening currents have on the total flux Φ, which in turn affects I_s in equation 1.22. We will now simplify the expression above by considering the limiting case for small currents, i.e. $I_\mathrm{s} \ll 2I_\mathrm{c}$. This condition implies that $\sin\varphi_1 \approx -\sin\varphi_2$ and thus $\varphi_1 \approx -\varphi_2$, leading to a vanishing cosine argument $\varphi_1 + \pi\frac{\Phi}{\Phi_0} \approx 0$. This results in

$$\Phi = \Phi_\mathrm{e} - \frac{1}{2}\beta_\mathrm{L}\Phi_0\sin\left(\pi\frac{\Phi}{\Phi_0}\right) \quad . \tag{1.26}$$

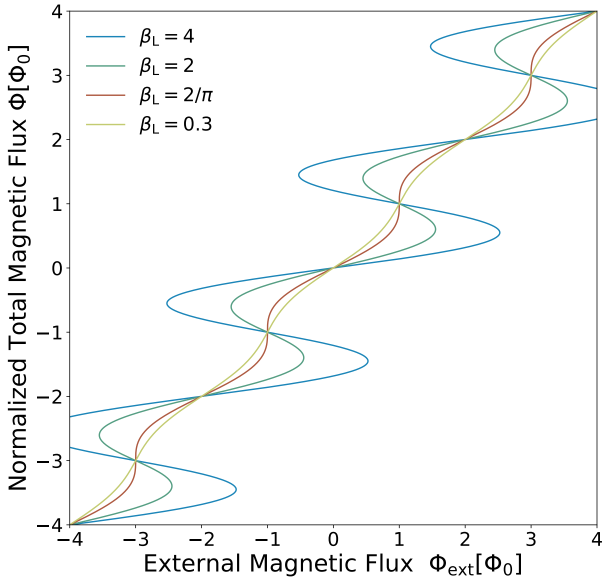

Figure 1.8: Normalized flux Φ modulated by the external flux Φ_e. The amplitude of the modulation depends on the screening parameter β_L, where $\Phi(\Phi_e)$ remains a single-valued function for $\beta_L \leq 2/\pi$.

Figure 1.8 showcases this relation for several values of β_L. High values ($\beta_L > 2/\pi$) correspond to hysteretic characteristics, meaning there can be multiple values of total flux Φ for the same applied flux Φ_e. For practical dc-SQUIDs, it is therefore desirable to avoid this ambiguous behavior. The intersections of each curve represents the case for $\Phi = n\Phi_0$, such that the screening currents vanish and the total flux equals the external flux ($\Phi = \Phi_e$). This is to be expected as the flux in a superconducting ring tends to be quantized (see equation 1.2). Consequently, the SQUID tries to maintain the total flux at integer values of Φ_0 for the limiting case of $\beta_L \gg 1$, where Φ_{cir} dominates over any applied flux. This compensation is visualized by the strong modulation for high β_L in figure 1.8, where a wide range of Φ_e values remain in the proximity of $n\Phi$. The other limiting case, i.e. $\beta_L \ll 1$, allows us to neglect the circulating currents such that we can write $\Phi \approx \Phi_e$. From equation 1.22 we then obtain the maximum possible supercurrent

$$I_s^m(\Phi_e) = 2I_c \left|\cos\left(\pi\frac{\Phi_e}{\Phi_0}\right)\right| \quad . \tag{1.27}$$

The modulation of this current quickly diminishes for increasing β_L, as was derived in [Cla04] to

$$\frac{\Delta I_s^m(\Phi_e)}{2I_c} \approx 1 - \frac{2\Phi_e}{\Phi_0\beta_L} \quad . \tag{1.28}$$

For the SQUIDs produced within the scope of this thesis, values of $\beta_L \approx 1$ were cosidered optimal to minimize resonant behavior without reducing the SQUID inductance L_s too much. In subsection 1.2.3 we will discuss how various parameters are chosen to ensure an optimal SQUID performance.

1.2.2 Voltage State

To utilize dc-SQUIDs as sensitive magnetometers, it is necessary to operate them in the voltage state by applying a large enough current bias I_b, such that $I_\mathrm{b} > 2I_\mathrm{c}$. In the case of negligible screening ($\beta_\mathrm{L} \ll 1, \Phi \approx \Phi_\mathrm{e}$) and strong damping ($\beta_\mathrm{c} \ll 1$), i.e. by chosing a small junction capacitance C and SQUID inductance L_s, it is possible to derive the flux dependency of the resulting voltage drop across the SQUID. Following the RCSJ model, we are only left with the supercurrent I_s and the resistive current I_n, such that by using equation 1.22 we can write for the bias current

$$I_\mathrm{b} = 2I_\mathrm{c}\cos\left(\pi\frac{\Phi_\mathrm{e}}{\Phi_0}\right)\sin\left(\varphi_1 + \pi\frac{\Phi_\mathrm{e}}{\Phi_0}\right) + 2\frac{V_\mathrm{s}}{R} \quad , \tag{1.29}$$

where we again assumed identical junctions, each shunted by a small shunt resistor $R_\mathrm{s} \ll R_\mathrm{n}$. Here R_n denotes the normal resistance of a single, unshunted junction. Therefore the total normal resistance R for each parallel connection is approximately $R \approx R_\mathrm{s}$. Additionally, we can define a new phase $\varphi = \varphi_1 + \pi\frac{\Phi}{\Phi_0}$ and with the maximum supercurrent from equation 1.27 we obtain a current relation that resembles that of a single junction:

$$I_\mathrm{b} = I_\mathrm{s}^\mathrm{m}(\Phi_\mathrm{e})\sin(\varphi) + \frac{2}{R_\mathrm{s}}\frac{\Phi_0}{2\pi}\frac{\partial\varphi}{\partial t} \quad . \tag{1.30}$$

This equivalence of a dc-SQUID and a single junction stems from the above-mentioned fact that the SQUID loop represents a single Josephson contact that provides a larger effective area external fields can penetrate. It is therefore possible to derive the voltage drop across the SQUID in the same manner as in subsection 1.1.3. With the critical current $I_\mathrm{s}^\mathrm{m}(\Phi_\mathrm{e})$ now being flux-dependent with a modulation of Φ_0, we compare with equation 1.19 and obtain for the time averaged voltage [Cla04]

$$\langle V(t)\rangle = \frac{R_\mathrm{s}}{2}\sqrt{I_\mathrm{b}^2 - I_\mathrm{s}^\mathrm{m}(\Phi_\mathrm{e})^2} \tag{1.31}$$

$$= I_\mathrm{c}R_\mathrm{s}\sqrt{\left(\frac{I_\mathrm{b}}{2I_\mathrm{c}}\right)^2 - \left[\cos\left(\pi\frac{\Phi_\mathrm{e}}{\Phi_0}\right)\right]^2} \quad . \tag{1.32}$$

Evidently, both the current and the voltage are flux dependent and are modulated by Φ_0. Figure 1.9 (left) showcases this behavior by considering the case for the minimum and maximum critical current, i.e. for $\Phi_\mathrm{e} = n\Phi_0$ and $\Phi_\mathrm{e} = (n + \frac{1}{2})\Phi_0$,

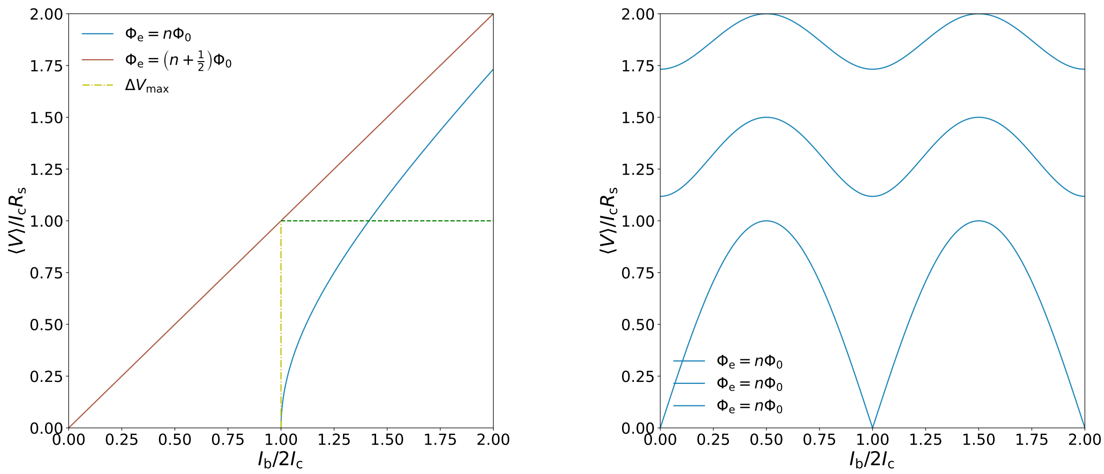

Figure 1.9: Left: IV-characteristics for a integer and half integer number of flux quanta for the limiting case of $\beta_c \ll 1$ and $\beta_L \ll 1$. The maximum voltage swing ΔV_{max} is approximately at $I_b \approx 2I_c$ and corresponds to $I_c R_s$ for a resistively shunted dc-SQUID. Right: The projection of equation 1.31 onto the $V\Phi$-plane shows the flux dependency of the voltage at various bias current values ($I_b \geq 2I_c$). The amplitude of the modulation decreases for increasing I_b.

with $n \in \mathbb{Z}$. The current-voltage-characteristics at these flux values are particularly interesting, as they can be used to extract crucial SQUID parameters like the voltage swing ΔV_{max}. This property describes how the voltage varies with the applied flux Φ_e, at a given current I_b. It is maximal at $I_b \approx 2I_c$, as depicted in figure 1.9 (right).

It is, however, important to note that equation 1.31 doesn't hold for practical SQUIDs, as they are typically not fabricated to fulfill the limiting case of $\beta_c \ll 1$ and $\beta_L \ll 1$. The conclusions reached here will nevertheless be applicable to practical SQUIDS, only needing a few adjustments.

1.2.3 Optimal Parameters

Negligible screening is not reasonable, as it would require to choose an extremely small SQUID inductance L_s, which in turn deteriorates the sensitivity for magnetic fields. The main reason to construct a dc-SQUID was to obtain a highly sensitive magnetometer by creating a large area for magnetic fields to thread through. Also, the fabrication process doesn't allow to produce an arbitrarily small junction capacitance C. The parameter β_c will therefore reach a lower limit as well, since also decreasing R_s too much reduces the voltage swing and increases the current white noise and energy sensitivity, as we will see in the following discussion. Now by allowing displacement and fluctuation currents, the current and voltage expressions become analytically unsolvable and therefore have to be solved numerically. In [?] such numerical simulations lead to optimal values of $\beta_c \approx 1$ and $\beta_L \approx 1$ to minimize the energy sensitivity.

To further fine-tune various parameters it is essential to look at how dc-SQUIDs are typically operated to achieve the highest possible flux sensitivity. Here, we distinguish between a current and a voltage bias, where the former was assumed in figure 1.9. Maximizing sensitivity in this mode is done by maintaining the flux thorugh a constant offset at the steepest point in the $V\Phi$-curve, which is referred to as the working point and corresponds to $\Phi_e = (2n+1)\frac{\Phi_0}{4}$. This allows for the largest possible voltage change ΔV at a given flux change $\Delta\Phi$. Similarly, at a voltage bias the working point will mark the steepest point in the $I\Phi$-curve. To quantify this, we will introduce the transfer parameters

$$V_\Phi \equiv \left| \left(\frac{\partial V}{\partial \Phi_e} \right) \right| \tag{1.33}$$

$$I_\Phi \equiv \left| \left(\frac{\partial I}{\partial \Phi_e} \right) \right| \quad . \tag{1.34}$$

As mentioned above, at $I_b \approx 2I_c$ (current bias) the amplitude of the voltage modulation is maximal. This needs to be modified for practical SQUIDs, where thermal fluctuations can't be neglected. The resulting thermal current I_{th} causes a rounding of the edge at $I_b = 2I_c$ (figure 1.9 (left)), thereby reducing ΔV_{max} and V_Φ [?]. To minimize this effect, numerical simulations were made that lead to the condition [?]

$$\frac{I_c}{5} \geq I_{th} \equiv \frac{2\pi k_B T}{\Phi_0} \quad . \tag{1.35}$$

A lower bound for I_c at $T = 4.2\,\mathrm{K}$ will therefore be approximately $1\,\mu\mathrm{A}$. This effect shifts the current $I_{b,max}$, at which the voltage swing is maximal, according to [?] by a temperature correction factor leading to

$$I_{b,max} \approx 2I_c(1 - \sqrt{\Gamma/\pi}) \quad , \tag{1.36}$$

where Γ is the noise parameter defined as $\Gamma = I_{th}/I_c$. Lastly, the thermal current can also be used to set an upper limit to the SQUID inductance. We can define a thermal inductance $L_{th} = \frac{\Phi_0}{2I_{th}}$ for the thermal current inducing half a flux quantum.

This should be significantly larger than the SQUID inductance L_s to minimize the impact of these thermal fluctuations. Again, simulations provided a constraint for optimization, giving the relation [**?**]

$$5L_\mathrm{s} \leq L_\mathrm{th} \equiv \frac{\Phi_0}{2I_\mathrm{th}} = \frac{{\Phi_0}^2}{4\pi k_\mathrm{B} T} \quad . \tag{1.37}$$

For $T = 4.2\,\mathrm{K}$ we would obtain $L_\mathrm{s} \leq 1\,\mathrm{nH}$, which is typically fulfilled for practical dc-SQUIDs.

1.2.4 Noise

The above-mentioned energy sensitivity, also called spectral noise energy density or energy resolution, is defined as the flux noise per SQUID inductance L_s and is typically expressed through a power spectral density as

$$\epsilon(f) = \frac{S_\Phi(f)}{2L_\mathrm{s}} \quad . \tag{1.38}$$

$$S_\Phi(f) = \frac{S_\mathrm{V}(f)}{V_\Phi^2} \tag{1.39}$$

$$S_\mathrm{V}(f) = \frac{4k_\mathrm{B}T}{R_\mathrm{s}} \left[2R_\mathrm{dyn}^2 + \frac{L_\mathrm{s}^2 V_\Phi^2}{2} \right] \tag{1.40}$$

$$S_\mathrm{V}(f) = 18 k_\mathrm{B} T R_\mathrm{s} \tag{1.41}$$

$$\epsilon(f) = 16 k_\mathrm{B} T \sqrt{L_\mathrm{s} C} \tag{1.42}$$

1.2.5 Parasitic Resonances

2. Experimental Setup

2.1 Practical dc-SQUIDs

2.2 Operation of a dc-SQUID

2.2.1 Flux-Locked Loop

2.2.2 Two-Stage Configuration

2.3 Metallic Magnetic Microcalorimeters

2.4 dc-SQUID Design

2.4.1 dc-SQUID with a Two-Turn Input Coil

2.4.2 Integrated Two-Stage Chip

2.4.3 Damping Methods

3. Experimental Results

3.1 dc-SQUID Parameters

3.1.1 Characteristic Quantities

3.1.2 Input Coil Inductance

3.1.3 Noise Performance

3.2 Integrated Two-Stage Measurements

3.2.1 General Properties

3.2.2 Noise Performance

4. Summary

Bibliography

[Bar57] J. Bardeen, L. N. Cooper, and J. R. Schrieffer, Theory of Superconductivity, *Phys. Rev.*, **108**(5), 1175–1204, 1957.

[Cla04] J. Clarke and A. I. Braginski (Ed.), *The SQUID Handbook: Vol. 1, Fundamentals and Technology of SQUIDs and SQUID Systems*, Wiley-VCH, 2004.

[Gin50] V. L. Ginzburg and L. Landau, On the theory of superconductivity, *Zh. Èksper. Teoret. Fiz.*, **20**, 1064–1082, 1950.

[Gro16] R. Gross, A. Marx, and F. Deppe, *Applied Superconductivity: Josephson Effect and Superconducting Electronics*, De Gruyter Textbook Series, Walter De Gruyter Incorporated, 2016.

[Ina80] Akira Inaba, Superconductive transition point of tantalum and niobium as a reference temperature, *Japanese Journal of Applied Physics*, **19**(8), 1553, 1980.

[Jos62] B. D. Josephson, Possible new effects in superconductive tunnelling, *Physics Letters*, **1**(7), 251–253, 1962.

[Jos65] B. D. Josephson, Supercurrents through barriers, *Advances in Physics*, **14**(56), 419–451, 1965.

[Lik86] K. K. Likharev, *Dynamics of Josephson Junctions and Circuits*, Gordon and Breach, New York, 1986.

[McC68] D. E. McCumber, Effect of ac Impedance on dc Voltage-Current Characteristics of Superconductor Weak-Link Junctions, *Journal of Applied Physics*, **39**(7), 3113–3118, 1968.

[Mei33] W. Meissner and R. Ochsenfeld, Ein neuer Effekt bei Eintritt der Supraleitfähigkeit, *Naturwissenschaften*, **21**(44), 787–788, 1933.

[Ste68] W. C. Stewart, Current-Voltage Characteristics of Josephson Junctions, *Applied Physics Letters*, **12**(8), 277–280, 1968.

[Tie21] Eite Tiesinga, Peter J. Mohr, David B. Newell, and Barry N. Taylor, Codata recommended values of the fundamental physical constants: 2018, *Rev. Mod. Phys.*, **93**, 025010, 2021.